Partial Volume Segmentation of Medical Images

Xiang Li, *Member, IEEE*, Daria Eremina, Lihong Li, *Member, IEEE,* and Zhengrong Liang, *Member, IEEE*

Abstract — **Image segmentation plays an important role in medical image processing. The aim of conventional hard segmentation methods is to assign a unique label to each voxel. However, due to the limited spatial resolution of medical imaging equipment and the complex anatomic structure of soft tissues, a single voxel in a medical image may be composed of several tissue types, which is called partial volume (PV) effect. Using the hard segmentation methods, the PV effect can substantially decrease the accuracy of quantitative measurements and the quality of visualizing different tissues. In this paper, instead of labeling each voxel with a unique label or tissue type, the percentage of different tissues within each voxel, which we call a mixture, was considered in establishing an image segmentation framework of maximum *a posterior* (MAP) probability. A new Markov random field (MRF) model was used to reflect the spatial information for the tissue mixture. Parameters of each tissue class were estimated through the expectation-maximization (EM) algorithm during the MAP tissue mixture segmentation. The MAP-EM mixture segmentation methodology was tested by digital phantom MR and patient CT images with PV effect evaluation. Results demonstrated that a hard segmentation method would loss a significant amount of details along the tissue boundaries, while the presented new PV segmentation method can dramatically improve the performance of preserving the details.**

I. Introduction

Image segmentation plays an important role in medical image processing, especially in quantitative analysis and visualization of normal and abnormal soft tissues. In the past decades, many image segmentation methods have been proposed and tremendous success has been achieved [1-4]. However, most of them belong to the category of hard segmentation, in which each voxel is classified as a single tissue type. Due to the limited spatial resolution of imaging devices and the complex anatomical structure of the tissues, there are frequently some voxels in the images that contain not only one tissue type, but rather a mixture of two or more tissue types. This is called partial volume (PV) effect. In the PV segmentation methods proposed by Choi *et al* [5] and others, the variance of the image noise was assumed as a constant, which is not valid and affects the accuracy of PV segmentation. In addition, the estimation of the mean parameter of each class is not sufficiently accurate with a stationary noise model as mentioned in their papers. Recently, Leemput *et al* [6] proposed an alternative PV model, in which the intensity of each class k is normally distributed with mean μ_k and covariance Σ_k and the intensity of each voxel is considered as the sum of the intensities of the sub-voxels from the down-sampled image, which is also Gaussian distributed. However, they assumed that there are at most two tissue types within each voxel, which is not often the case for the medical imaging studies and furthermore it is very difficult to determine which tissue types in a specific voxle if there are more than two tissue types in the whole volume. In this paper, we adopted the PV model proposed by Leemput and utilized a *Markov random field* (MRF) spatial prior function to perform tissue mixture segmentation by the *maximum a posterior probability* (MAP) criterion, where the *expectation-maximization* (EM) algorithm [7] was employed for estimation of the model parameters.

Manuscript submitted on October 19, 2003. This work was supported in part by the NIH National Heart, Lung and Blood Institute under Grant No. HL54166 and the NIH National Cancer Institute under Grant No. CA82402.

X. Li is with the Department of Radiology, State University of New York, Stony Brook, NY, 11794, USA (telephone: 631-444-7921, e-mail: xli@mil.sunysb.edu).

D. Eremina is with the Departments of Applied Mathematics and Radiology, State University of New York, Stony Brook, NY 11794, USA.

L. Li is with the Department of Radiology, State University of New York, Stony Brook, NY 11794, USA.

Z. Liang is with the Departments of Radiology and Computer Science, State University of New York, Stony Brook, NY 11794, USA.

II. Theory

A. PV Image Model

Let Γ and S be two sets: $\Gamma = \{1,2,\cdots,K\}$, and $S = \{1,2,\cdots,N\}$, where K is the total number of tissue classes and N is the total number of voxels in the acquired image. Let $\boldsymbol{Y}$ be a set of random variables, which represent the observed image intensities $Y = \{y_1,\cdots,y_i,\cdots y_N \,|\, i \in S\}$, and M be a set of vectors $M = \{m_1,\cdots,m_i,\cdots,m_N \,|\, i \in S\}$ with the following properties of (a) $m_i = (m_{i1},\ldots,m_{ik})$, $k \in \Gamma$, and (b) $\sum_{k=1}^{K} m_{ik} = 1$, $0 \le m_{ik} \le 1$, where m_{ik} reflects the fraction of tissue type k inside voxel i. Each voxel value y_i in the observed image is considered as the following random process:

$$y_i = \sum_{k=1}^{K} m_{ik}\mu_k + \varepsilon_i \qquad (1)$$

where μ_k is the observed mean value of tissue type or class k when it fully fills in a voxel; m_{ik} can be defined as the probability of voxel i belonging to class k [8]; and ε_i is assumed as Gaussian noise associated with the observation

y_i at voxel *i* with its mean being zero and variance of ν_i. In the multi-spectral magnetic resonance imaging (MRI) situation, ν_i becomes a covariance matrix Σ_i, which can be assumed to be a diagonal matrix if there are no correlations between different modality images, such as the acquired T_1 and T_2 weighted MR images by different RF pulse sequences.

B. PV Image Segmentation

In order to estimate the mixture vectors *M*, given the observed image ***Y***, the statistically optimal MAP principle is used. We assume that the observation at each voxel is independent from the observations of other voxels, while the underline tissue distribution follows a MRF process, so that the conditional probability of the observed image ***Y***, given mixture *M*, can be simply expressed as

$$P(Y|M,\Phi)=\prod_{i=1}^{N} p(y_i|m_i,\Phi) \\ =\prod_{i=1}^{N}(\frac{1}{2\pi})^{\frac{r}{2}}|\Sigma_i|^{-\frac{1}{2}}\exp[-\frac{1}{2}(y_i-\mu^T m_i)^T\Sigma_i^{-1}(y_i-\mu^T m_i)] \quad (2)$$

where Φ is the parameter set $\{\mu_k,\Sigma_i,k\in\Gamma,i\in S\}$ and *r* is the number of different modality images, for example, *r* should be 3 if T_1, T_2 and Flair MR images are used [1].

According to the MAP principle, the PV segmentation

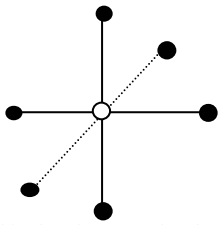

Figure1. The neighborhood system sketch, where the empty circle represents the present voxel and the solid circles are the neighborhood voxels.

can be achieved by maximizing the posterior distribution, which is proportional to the joint distribution

$$P(M|Y,\Phi)=\frac{P(Y|M,\Phi)P(M|\Phi)}{P(Y|\Phi)}\propto P(Y|M,\Phi)P(M|\Phi) \quad (3)$$

where a MRF model has been used to define the prior distribution of mixture *M*,

$$p(m_i|N_i)=\frac{1}{Z}\exp(-\alpha\sum_{j\in N_i}\kappa_j\|m_i-m_j\|^2) \quad (4)$$

where N_i denotes the neighborhood of voxel *i*, α is a parameter controlling the degree of the smooth penalty on the mixture *M*, κ_j is a scale factor reflecting the difference among different orders of the neighbors, and *Z* is the normalization factor for the MRF model. In this paper, only the first-order neighborhood system was used as shown in Figure1.

In searching for the solution for maximizing the posterior probability of equation (3), the well-established iterated conditional modes (ICM) algorithm was utilized in this paper. Equivalently, the solution is determined by minimizing the posterior energy function of

$$U=\frac{1}{2}[y_i-\mu^T m_i]^T\Sigma_i^{-1}[y_i-\mu^T m_i]+\alpha\sum_{j\in N_i}\kappa_j\|m_i-m_j\|^2 . \quad (5)$$

Equation (5) has a quadratic property. So we can rewrite it as follows

$$U=\frac{1}{2}m_i^T A m_i+b^T m_i+C \quad (6)$$

$$A=[\mu\Sigma_i^{-1}\mu^T+2\alpha\sum_{j\in N_i}\kappa_j I] \quad (7)$$

$$b^T=-y_i^T\Sigma_i^{-1}\mu^T-2\alpha\sum_{j\in N_i}\kappa_j m_j^T \quad (8)$$

where *C* is a constant and *I* is an identity matrix. Given the smoothing properties of mixture m_i, the solution of minimizing function (5) is unique.

Performance of the PV segmentation on minimizing equation (5) strongly depends on an accurate estimation of the model parameter set Φ or (μ_k, Σ_i). In the next section, we employ the EM algorithm [7] to estimate the model parameters Φ.

C. Parameter Estimation

Within each voxel volume, there are possibly *K* tissue types, where each tissue type has a contribution to that observed voxel value y_i. Let x_{ik} be the contribution of tissue type *k* to the observation y_i. Assuming that x_{ik} follows a Gaussian distribution and all tissue types are not correlated each other, we have the following equation of

$$y_i=\sum_{k=1}^{K} x_{ik} . \quad (9)$$

The conditional probability of x_{ik} given the parameter set Φ is distributed following a normal functional $N(m_{ik}\mu_k, m_{ik}\sigma_k)$, where σ_k is the variance of observing tissue type *k* when it fully fills a voxel. This σ_k definition implies that the variance ν_i of observing the mixture voxels is smooth over the whole image volume and has the following property of $\nu_i=\sum_{k=1}^{K} m_{ik}\sigma_k$ for each voxel *i*. When voxel *i* is fully filled by a same tissue type *k*, then $\nu_i=\sigma_k$. A similar definition for the relation of ν_i and σ_k,

as well as the probability function for x_{ik}, were reported in Leemput's work in terms of down sampling [6].

By the EM terminology, an observation y_i is a random variable, which is incomplete in reflecting the underline true information, while x_{ik} is an unobservable random variable and reflects the complete information for each underline tissue process. The EM algorithm seeks a solution for the model parameters Φ, now they include both μ_k and σ_k, via the complete sampling density by interleaved Expectation and Maximization steps in an iterative manner.

The E-step computes the conditional complete-sampling density, given the observed data $\boldsymbol{Y}$ and the n-th iterated estimate of the model parameter $\Phi^{(n)}$

$$Q(\Phi|\Phi^{(n)}) = \mathrm{E}[\ln P(\mathbf{X}|\Phi)|\mathbf{Y},\Phi^{(n)}] = -\frac{1}{2}\sum_{i,k}[\ln(2\pi)+\ln(m_{ik}\sigma_k)+\frac{1}{m_{ik}\sigma_k}(x_{ik}^{2(n)}-2m_{ik}\mu_k x_{ik}^{(n)}+m_{ik}^2\mu_k^2)], \quad (10)$$

where the conditional means for x_{ik} and x_{ik}^2 are given below

$$x_{ik}^{(n)} = \mathrm{E}[x_{ik}|y_i,\Phi^{(n)}] = m_{ik}\mu_k^{(n)} + \frac{m_{ik}\sigma_k^{(n)}}{\sum_{j=1}^{K} m_{ij}\sigma_j^{(n)}}\cdot(y_i - \sum_{j=1}^{K} m_{ij}\mu_j^{(n)}) \quad (11)$$

$$x_{ik}^{2(n)} = \mathrm{E}[x_{ik}^2|y_i,\Phi^{(n)}] = x_{ik}^{(n)2} + m_{ik}\sigma_k^{(n)}\frac{\sum_{j\neq k}^{K} m_{ij}\sigma_j^{(n)}}{\sum_{j=1}^{K} m_{ij}\sigma_j^{(n)}} \quad (12)$$

The M-step determines the (n+1)-th iterated estimate, which maximizes the conditional complete-sampling density of equation (10).

For parameter μ_k we have:

$$\frac{\partial Q(\Phi|\Phi^{(n)})}{\partial \mu_k}\Big|_{(n+1)} = 0 \quad (13)$$

which results in

$$\mu_k^{(n+1)} = \frac{\sum_i x_{ik}^{(n)}}{\sum_i m_{ik}}. \quad (14)$$

For parameter σ_k, we have:

$$\frac{\partial Q(\Phi|\Phi^{(n)})}{\partial \sigma_k}\Big|_{(n+1)} = 0 \quad (15)$$

which results in

$$\sigma_k^{(n+1)} = \frac{1}{N}\sum_i \frac{(x_{ik}^{2(n)} - 2m_{ik}\mu_k^{(n+1)}x_{ik}^{(n)} + m_{ik}^2\mu_k^{(n+1)2})}{m_{ik}} = \frac{1}{N}\sum_i \{m_{ik}[\mu_k^{(n)} - \mu_k^{(n+1)} + \frac{\sigma_k^{(n)}(y_i - \sum_{j=1}^{K} m_{ij}\mu_j^{(n)})}{\sum_{j=1}^{K} m_{ij}\sigma_j^{(n)}}]^2 + \frac{\sigma_k^{(n)}\sum_{j\neq k}^{K} m_{ij}\sigma_j^{(n)}}{\sum_{j=1}^{K} m_{ij}\sigma_j^{(n)}}\} \quad (16)$$

III. RESULTS

The presented new PV segmentation algorithm was first tested by simulated MRI brain phantom images obtained from the Brain Web Simulation Database at the McConell Brain Imaging Center of the Montreal Neurological Institute, McGill University [10], which has been widely used to evaluate the hard segmentation algorithms. In this study, we employed the T_1 image with 3% noise to evaluate our new algorithm. The whole image volume was classified into three classes: white matter (WM), gray matter (GM) and cerebral-spinal fluid (CSF). Since the ground truth for this digital phantom is a kind of hard segmentation, both the conventional hard segmentation algorithms and our PV segmentation are therefore expected to have a similar performance. To compare with the non-mixture ground truth, our PV segmentation results were transferred into hard segmentation by labeling each voxel with a tissue type, which indicates that this voxel has the highest probability belonging to that class.

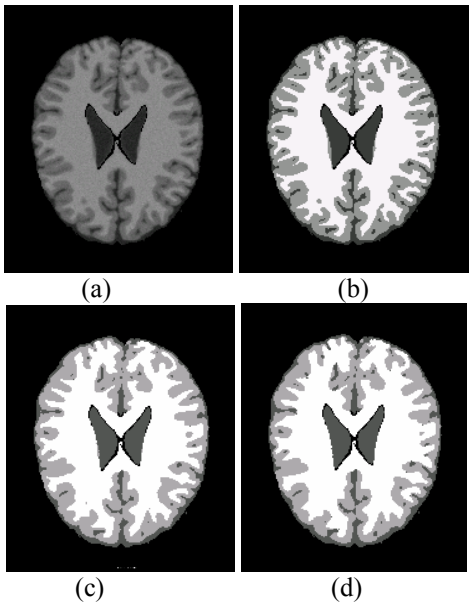

Figure2. Digital phantom study: (a) T_1 image, (b) ground truth, (c) hard segmentation, and (d) PV segmentation.

Figures 2(a)-(d) show the MR phantom T_1 image -- 2(a), the non-mixture ground truth -- 2(b), the MAP-MRF-based hard segmentation [1] -- 2(c), and our new PV segmentation -- 2(d), respectively. Compared with the ground truth in Figure 2(b), both the hard and PV segmentations show very good and similar results by visual judgment, as expected. In order to see more details, two merits were used to perform a quantitative comparison: true positive fraction (TPF) and false positive fraction (FPF), which are defined as follows:

$$TPF = \frac{Volume_{seg}^{+} \cap Volume_{groundtruth}^{+}}{Volume_{groundtruth}^{+}} \times 100\% \quad (17)$$

$$FPF = \frac{Volume^{-}_{seg} \bigcap Volume^{+}_{groundtruth}}{Volume^{+}_{groundtruth}} \times 100\% \quad (18)$$

where sign + or – represents that a voxel belongs to a specific tissue or not. Obviously, a perfect segmentation has a TPF being one and FPF of zero.

Table1 below shows the quantitative comparison results between the conventional MAP-MRF-based hard segmentation and our new PV segmentation. Both methods have a very good and similar performance for the designed non-mixture phantom test image, as expected. The conventional MAP-based hard segmentation has a slightly better performance than our new PV segmentation, because of the designed non-mixture phantom test image. This is a reasonable result, because the test image used here does not take into account the PV effect and fits the conventional MAP-MRF-based hard segmentation method.

Table 1. Quantitative comparison of different methods

	WM		GM		CSF	
	TPF	FPF	TPF	FPF	TPF	FPF
MRF	95.2	2.49	95.8	5.48	95.4	5.59
PV	95.4	5.80	93.4	6.68	92.2	5.62

As a matter of fact, there is a very strong PV effect in the clinical medical images [11]. In order to evaluate the accuracy of our new PV segmentation method, we modified the MR phantom test image with PV effect, based on the ground truth as shown in Figure 3(b). In the ground truth, there is exactly one tissue type within each voxel. There are totally three classes: WM, GM and CSF. First, we generated, based on the ground truth, three images for each class, in which the intensity of each voxel was set to 1 if this voxel belongs to the specific tissue, otherwise 0. Secondly, a low-pass Gaussian filter was applied to each of the three single-tissue images to produce the ground truth for the PV effect, which reflects the mixture value for each class. It is well-known that the noise model in MR images can be regarded as tissue-dependent, therefore, we set the class or model parameters as seen in the first row in Table 2. Finally, based on the PV-effect ground truth, we simulated the noisy MR image with PV effect as shown in Figure 3(a).

Table 2. Parameter estimation of each class

	WM		GM		CSF	
	mean	var	mean	var	mean	var
simulation	140.0	49.0	80.0	9.0	50.0	25.0
estimation	142.9	47.3	82.1	11.3	47.7	23.9

Both the MAP-based hard segmentation algorithm [1] and our new PV segmentation method were applied to the simulated noisy MR image with PV effects. Figure 3(c) shows the hard segmentation result. It was clearly seen that the hard segmentation misses a significant details along the boundaries. Figures 3(d), 3(e) and 3(f) show the mixture of CSF, GM and WM, respectively. Compared with the hard segmentation, the results obtained by our PV segmentation method reflect a more accurate anatomic structure. In order to quantitatively evaluate the accuracy of our new PV segmentation method, the difference images for each class between the segmented mixtures of our new method and the ground truth were shown in Figures 3(g), 3(h) and 3(i), have intensity values of 256 gray levels. For the mixture image, white color represents the gray value 1 (100% belonging to this tissue type) and black color respectively. It is noted that all the three difference figures represents the gray value

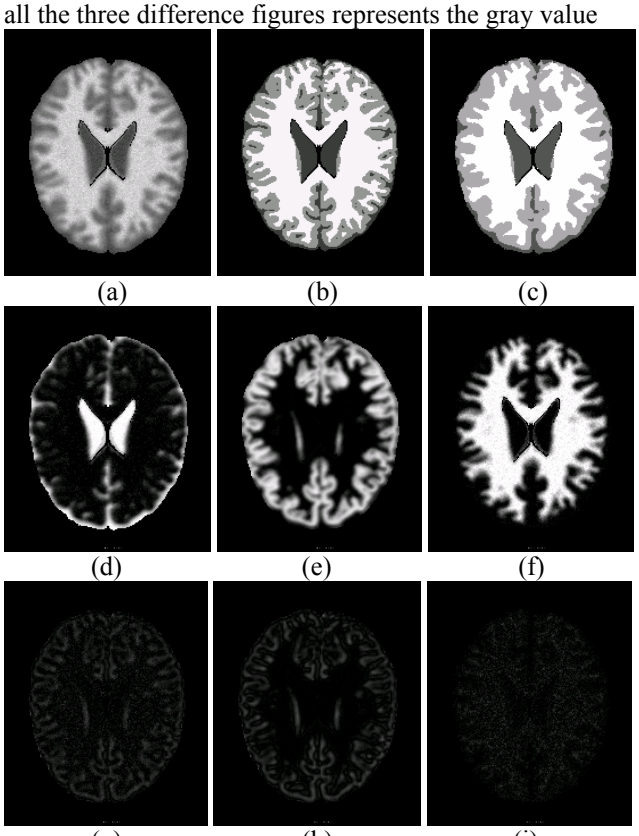

Figure 3. Partial volume effect simulation study results: (a) is the simulated mixture MR image from the ground truth (b); (c) shows the MAP-MRF hard segmentation with missing of a significant details along the boundaries; (d) is the PV mixture segmentation of CSF; (e) is the PV mixture segmentation of GM; and (f) is the PV mixture segmentation of WM. Pictures (g), (h) and (i) are the difference images of the PV segmentations of CSF, GM and WM against their corresponding ground-truth, respectively.

0 (not belonging to this tissue type at all). For all the difference images, we used the same window setting parameter. Therefore, the darker a difference images is, the higher the accuracy of our PV segmentation is. All the difference images demonstrated that the error of our new PV segmentation is very small. In addition, the estimated tissue model parameters by our method were very accurate as shown in the second row of Table 2.

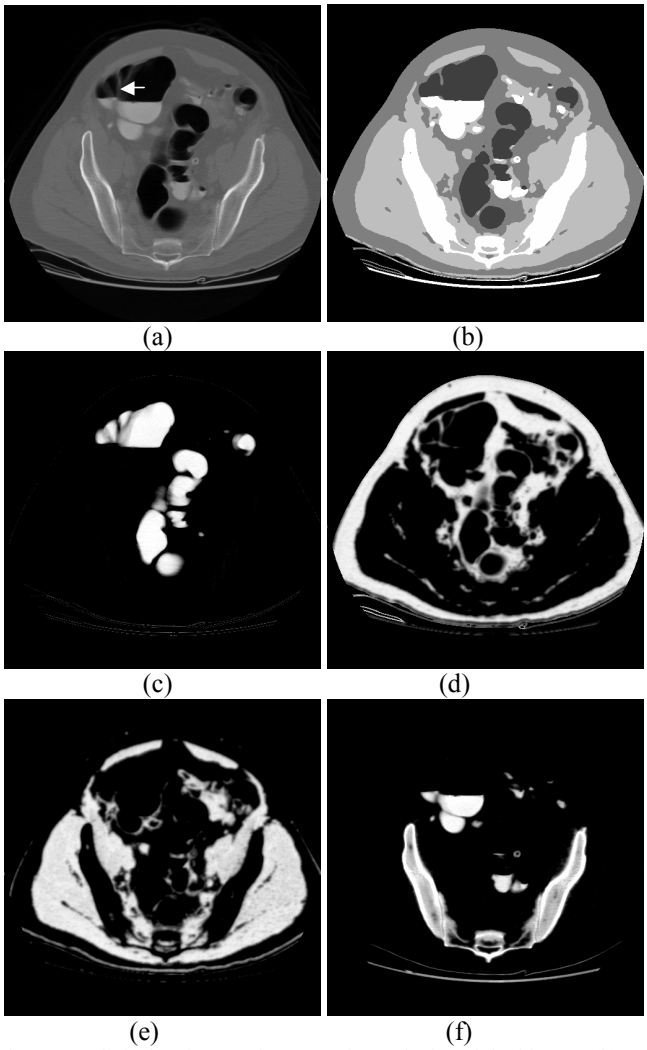

Figure 4. Clinical patient CT image study: (a) is the original image; (b) is the hard segmentation of four classes – are, soft tissue, muscle and bone. Pictures (c)-(f) are the mixture segmentations of the air, soft tissue, muscle and bone, respectively. A great amount of details of the classes are preserved in our PV segmentation as compared to the hard segmentation.

Finally, our new PV segmentation was applied to clinical CT (computed tomography) patient image. Figure 4(a) shows the CT image, which consists of four classes: air, soft tissue, muscle and bone. The MAP-MRF-based hard segmentation result is shown by Figure 4(b), in which it is clearly seen that a significant amount of details between air and soft tissue are missed. Figures 4(c), 4(d), 4(e) and 4(f) show the mixture segmentation of the air, soft tissue, muscle and bone, respectively. Compared with the hard segmentation, more structures are seen in our new PV segmentation by visual judgment. For example, the colon wall pointed by the arrow in Figure 4(a) is missed by the hard segmentation and is accurately detected by our new PV segmentation.

IV. Conclusions

A new MAP-MRF-based mixture PV segmentation algorithm was derived and tested by both simulated MR and clinical CT image datasets. The results demonstrated that our new PV segmentation method can detect the PV effects very well. When there are not PV effects in the images, our new PV segmentation showed almost the same performance, as expected, compared to conventional MAP-MRF-based hard segmentation, indicating that our method is theoretically equivalent to the MAP-MRF framework for non-mixture ground truth. In practical situations where PV effects are not avoidable, our method achieved a dramatically improvement over the hard segmentation of the well-established MAP-MRF framework.

V. References

[1]. Z. Liang, J. R. Macfall, and D. P. Harrington, "Parameter estimation and tissue segmentation from multispectral MR images," *IEEE Trans. Med. Imag*., vol. 13, pp. 441-449, Sept, 1994.

[2] Y. Zhang, M. Brady, and S. Smith, "Segmentation of brain MR images through a hidden markov random field model and expectation-maximization algorithm", *IEEE Trans. Med. Imag.*, vol. 20, pp. 45-57, 2001.

[3] W. M. Wells III, W. E. L. Grimson, R. Kikinis, and F. A. Jolesz, "Adaptive segmentation of MRI data", *IEEE Trans. Med. Imag.*, vol. 15, pp. 429-442, 1996.

[4] K. V. Leemput, F. Maes, D. Vandermeulen, and P. Suetens, "Automated model-based tissue classification of MR images of the brain," *IEEE Trans. Med. Imag.*, vol. 18, pp. 897-908, 1999.

[5] H. S. Choi, D. R. Haynor, and Y. Kim, "Partial volume tissue classification of multichannel magnetic resonance images- A mixel model," *IEEE Trans. Med. Imag*., vol. 10, pp. 395-407, Sept, 1991.

[6]. K. V. Leemput, F. Maes, D. Vandermeulen, and P. Suetens, "A unifying framework for partial volume segmentation of brain MR images," *IEEE Trans. Med. Imag*., vol. 22, pp. 105-119, Jan, 2003.

[7] A. Dempster, N. Laird, and D. Rubin, "Maximum likelihood from incomplete data via the EM algorithm", *J R Stat. Soc*., vol. 39B, pp. 1-38, 1977.

[8] Z. Liang, R. J. Jaszczak, and R. E. Coleman, "Parameter estimation of finite mixtures using the EM algorithm and information criteria with application to medical image processing," *IEEE Trans. Nucl. Sci.*, vol. 39, pp. 1126-1133, 1992.

[9] D. Chen, L. Li and Z. Liang, "A self-adaptive vector quantization algorithm for MR image segmentation", *Proc. Intl Society Magnetic Resonance Medicine*, 1999.

[10] C. A. Cocosco, V. Kollokian, R. K-S. Kwan, and A. C. Evans, "BrainWeb: Online interface to a 3D MRI simulated brain database", *NeuroImage*, vol.5, no.4, part 2/4, S425, 1997. http://www.bic.mni.mcgill.ca/brainweb/.

[11] W. J. Nissen, K. L. Vinclen, J. Weickert, B. M. ter Haar Romeny, and M. A. Viergever, "Multiscale segmentation of three-dimentional MR brain images", *Int. J.Comput.Vis*., vol.31, no. 2/3, pp. 185-202, 1999.